Special Issue on "Theoretical and Computational Chemistry"

J. Indian Chem. Soc.,
Vol. 96, July 2019, pp. 793-800

Ab initio study of hydrogen storage in lithium grafted metal-graphyne framework

Sandeep Kumar and T. J. Dhilip Kumar*

Department of Chemistry, Indian Institute of Technology Ropar, Rupnagar-140 001, Punjab, India

E-mail: dhilip@iitrpr.ac.in

Manuscript received online 28 April 2019, revised and accepted 13 May 2019

Hydrogen holds the promise to replace the widespread dependency on fossil fuels due to its renewable and pollution free nature. Metal-graphyne framework (MGF) constructed with magnesium oxide as a metal node and graphyne as a linker. Graphyne is a new 2D carbon allotrope connected with acetylenic linkages. Lithium is grafted on the graphyne linker of MGF. Density functional theory (DFT), with GGA-PBE exchange-correlation functional, is used to determine the geometric structures, their stability, binding strength of Li and graphyne of MGF, and hydrogen storage capacity. On full saturation with hydrogen, each Li atom physisorbs 3 H_2 molecules in the $MGFLi_{16}$ which results $MGFLi_{16}$-$48H_2$ system with a total gravimetric density of 7.2 wt.%. Further 12 more H_2 molecules could be accommodated in the pore space of $MGFLi_{16}$ and the resulting structure, $MOFLi_{16}$-$60H_2$ is obtained with hydrogen wt.% 8.9. The H_2 and Li interacted by Niu-Rao-Jena mechanism with average H-H bond distance enhanced up to 0.754 Å. The calculated sorption energies are found in the range of 0.36 to 0.21 eV. The molecular dynamics simulations reveal the stability of Li grafted MGF and the reversibility of adsorbed H_2 from the $MGFLi_{16}$-$48H_2$ system. The energetics and storage capacity meet the US DOE target which makes $MGFLi_{16}$ as a potential hydrogen storage material.

Keywords: Density functional theory, Li grafting, hydrogen storage, charge polarization, Born-Oppenheimer molecular dynamics.

Introduction

An everyday increase in the demand for energy and inadequate availability of energy resources makes hydrocarbon economy impractical. The conventional energy resources also release carbon dioxide which put an adverse effect on the environment[1,2]. Thus, the limited availability of fossil fuels and their harmful effect on the environment increases interest in the scientific community to replace the conventional energy economy with the environmental friendly hydrogen economy[1,3]. Hydrogen gas is considered as a carbonless economy as it is a clean and renewable carrier of energy[1–5]. However, hydrogen is not freely available which makes it necessary to generate, store and transport it to the desired places for its further use in various applications. Presently, physical and materials-based techniques are used to store hydrogen[2,3]. In physical based methods hydrogen is stored either in compressed form or in the form of liquified hydrogen. But these methods are not commercially feasible because they require expensive infrastructure and consume a large amount of energy during the storage. In material-based methods hydrogen can be stored in two ways viz. physical adsorption and chemical adsorption[2,3,6]. The storage of hydrogen via physical adsorption is found to be reversible which follows very fast kinetics as compared to the chemical adsorption pathway[6,7].

In recent years, a variety of materials have been studied and reported by several research groups which could be considered as hydrogen storage materials in the future. Nano porous materials such as carbon nanotubes[8], graphene[9], graphynes[10–15] and fullerenes[16] have been found to store hydrogen at ambient temperature and pressure conditions via associative manner. Several materials such as calix[n]-arenes[5,17–19], zeolites[20,21], metal-organic frameworks (MOFs)[22–27], covalent-organic frameworks (COFs)[28,29], metal-inorganic frameworks[30,31] and other materials[32,33] have also been explored as potential hydrogen storage materials. The current research is focused on designing novel hydrogen storage materials to achieve the targets which are set by the U.S. Department of Energy (US DOE)[34].

Among all the proposed porous materials, MOFs are extensively studied as hydrogen storage materials due to the availability of large surface area which further provides a large

number of binding sites for hydrogen molecules[35,36]. The objective of the present work is to design the metal-graphyne framework (MGF) by using magnesium oxide as a metal node and graphyne as a linker and explore the hydrogen storage capacity, reversibility and thermodynamic stability of Li grafted MGF. Graphyne is a 2D sheet of carbon allotrope first discovered by Baughman *et al.*[10]. In graphyne; benzene rings are connected by acetylenic linkages (-C-C≡C-C-). It is reported that metal decorated graphyne have been explored for hydrogen storage with high gravimetric density[38].

Recently, we designed and explored metal-graphyne framework consists of graphyne[27] linker decorated with lithium (MGF-Li_8) as a hydrogen storage material with the aid of density functional theoretical calculations. The computed molecular dynamics simulations results indicate the high reversibility of H_2 molecules in MGF-Li_8. Furthermore, the designed metal-graphyne framework decorated from one side with lithium are reported to store 6.4 wt% of hydrogen. In this work, the lithium is decorated on both sides of the metal-graphyne framework (MGF-Li_{16}) and studied the hydrogen storage capacity, reversibility and thermodynamic stability and the results are compared.

This paper is organized as follows: In next Section, computational details are presented. In the following Section, the results and discussions of hydrogen storage properties of Li grafted MGF are discussed. The summary and conclusions are provided in last Section.

Computational details

All the calculations are performed by density functional theory (DFT) with the spin-unrestricted method using the DMOL^3 code[39,40]. The Perdew-Burke-Ernzerhof (PBE) exchange-correlation functional within the spin-polarized generalized gradient-corrected approximation (GGA) is employed[41]. Double numerical basis set with polarization function (DNP) is adopted. The DFT-D (D stands for dispersion) approach with Grimme's van der Waals (vdW) correction term is used to determine the accurate description of weak interactions[42]. The real-space global orbital cutoff radius 5.2 Å is used for high quality results.

Energy parameters such as Li binding energy between Li and MGF, adsorption and desorption energy of adsorbed H_2 molecules, changes in bond lengths before and after the hydrogen adsorption, Hirshfeld charge analysis, thermodynamics of usable hydrogen storage and Born-Oppenheimer molecular dynamics (BOMD)[43] simulations have been studied.

The binding energy of Li of $MGFLi_{16}$ is determined by the following equation[44,45],

$$C_b = \frac{1}{16}\left[(16E_{Li} + E_{MGF}) - E_{MGFLi_{16}}\right] \quad (1)$$

where, $E_{MGFLi_{16}}$, is the total energy of $MGFLi_{16}$, E_{Li} energy of Li metal and E_{MGF} is the energy of MGF, respectively.

The average H_2 adsorption energy, E_{ad} is calculated by given equation[44,45],

$$E_{ad} = \frac{1}{n}\left[\left(E_{MGF_{16}} + nE_{H_2}\right) - E_{MGFLi_{16}\text{-}nH_2}\right] \quad (2)$$

where E_{H_2}, $E_{MGFLi_{16}\text{-}nH_2}$, and n are the energy of H_2 molecule, the energy of $MGFLi_{16}$ and number of adsorbed hydrogen molecules.

To calculate the sequential desorption energy of adsorbed hydrogen molecules, the given equation is used,

$$E_{de} = E_{H_2} + E_{MGFLi_{16}\text{-}(n\text{-}1)H_2} - E_{MGFLi_{16}\text{-}nH_2} \quad (3)$$

where $E_{MGFLi_{16}\text{-}(n\text{-}1)H_2}$ is represented total energy of preceding H_2 molecules adsorbed on $MGFLi_{16}$-nH_2 system.

N_{use} The practical usable hydrogen storage capacity has been determined by using chemical potential, μ at adsorbing (low temperature-high pressure) and desorbing (high temperature-low pressure) conditions. The thermodynamic usable hydrogen capacity is determined by calculating the occupation number (N_{use}) as,

$$N_{use} = \frac{\sum_{n?0}^{N_{Max}} n g_n \exp[n(\mu - E_{ad})/k_B T]}{\sum_{n=0}^{N_{Max}} g_n \exp[n(\mu - E_{ad})/k_B T]} \quad (4)$$

Here, N_{Max}, n, and g_n are the maximum numbers of adsorbed H_2 molecules per Li in $MGFLi_{16}$, a number of hydrogen molecules adsorbed and the configurational degeneracy of n, k_B is the Boltzmann constant, and E_{ad} represents the adsorption energy of hydrogen molecules stored in Li grafted MGF. The chemical potential, μ of gas phase H_2 at given pressure and temperature determined by the equation,

$$\mu = \mu_{ideal} - 0.00015(T - 186.5) + 0.00065[(\log P - 0.5)^2 - 0.25] \quad (5)$$

The gas phase chemical potential μ of H_2 gas as a function

of temperature and pressure is chosen from the experimental data[46,47].

The electron distribution and electron charge transfer mechanism are explained by using the Hirshfeld charge analysis. BOMD[43] simulations are performed to determine the stability of $MGFLi_{16}$ system, and the reversibility of adsorbed H_2 molecules from the Li grafted MGF. The BOMD simulations have been performed at the range of temperature with Γ-point sampling at 5 ps run time and 1 fs time-step. Canonical NVT ensemble uses with Nose thermostat to control the temperature during BOMD simulations.

Results and discussion

The structure of the MGF is optimized and provided in Fig. 1. MGF has been designed with graphyne linker and magnesium oxide as a metal node[27]. Each graphyne linker of MGF is grafted with 4 Li atoms, two Li used from the top, and other two from the bottom side and the resulting structure $MGFLi_{16}$ is represented in Fig. 2a. Li atoms are used in their ground state configuration to graft the MGF. The average Li binding energy in $MGFLi_{16}$ is calculated by using eq. (1) and is found to be 2.68 eV, which indicate that Li atoms strongly bind with graphyne linker of MGF. In MGF, the distance between a diagonal metal node to metal node and between adjacent metal nodes are 24.45 Å and 17.33 Å respectively. The geometry of $MGFLi_{16}$ shows that the distance between a diagonal metal node to metal node and between adjacent metal nodes are increasing and is found to be 24.55 and 17.39 Å on Li grafting of MGF.

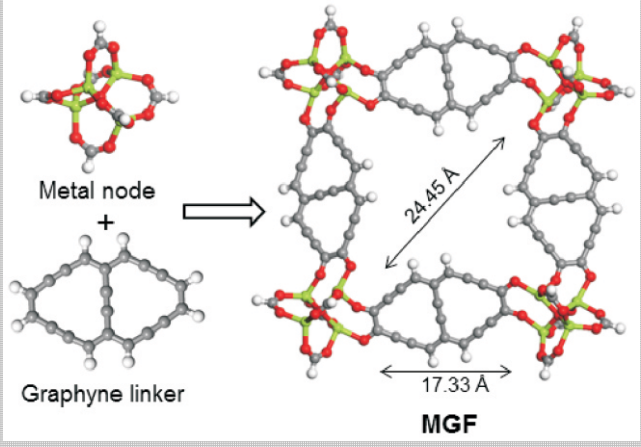

Fig. 1. Structure of metal-graphyne framework (MGF). Mg, C, H and O atoms are represented by green, dark grey, white and red colors respectively.

Structural changes on the adsorption of H_2 molecules in $MGFLi_{16}$

The H_2 molecules are subsequently introduced on each Li of optimized $MGFLi_{16}$. After optimization, it is observed that H_2 molecules on each Li in $MGFLi_{16}$-nH_2 system is adsorbed in a molecular manner with elongation in H-H bond distance up to 0.755 Å from its bare distance of 0.741 Å. On sequential adsorption of H_2 molecules shows that maximum three H_2 molecules is adsorbed on per Li in $MGFLi_{16}$ resulting $MGFLi_{16}$-$16H_2$, $MGFLi_{16}$-$32H_2$, and $MGFLi_{16}$-$48H_2$ systems. The H_2 adsorption cycle of $MGFLi_{16}$-nH_2 (where n = 16, 32, and 48) is represented in Fig. 2b-d. In Fig. 2a1, Li binding to the linker is shown enlarged. Similarly, in Fig. 2b1-d1, H_2 binding to the Li metals is shown enlarged. It is observed that all the H_2 molecules bind on each Li in $MGFLi_{16}$-nH_2 (where n = 16, 32, and 48) in molecular form. The H_2 molecules bind with Li in physisorbed fashion by Niu-Rao-Jena charge polarization mechanism[48,49]. In charge polarization mechanism, charge generates on graphyne linker, shifts to the Li atoms, the charge on Li atoms polarizes the incoming H_2 molecules in the system; as a result, H_2 molecules bind in molecular form. The molecular adsorption indicates that all the H_2 molecules are physisorbed on $MGFLi_{16}$-nH_2.

The Li-Li distance of the top and bottom of each linker increases from 2.547 to 2.749 Å with the number of H_2 molecules in the system. The distance between a diagonal metal node to metal node and between adjacent metal nodes decreases on the adsorption of first H_2 molecule on each Li in the system while on adsorption of second and third H_2 molecules on each Li in the system, both the distances increases as shown in hydrogen adsorption cycle in Fig. 2b-d. The distance between Li and center of graphyne linker (Li-Gc), and between Li and adsorbed H (Li-H) increases with the number of hydrogen molecules adsorbed in the $MGFLi_{16}$-nH_2 (n = 16, 32, and 48) system. The distance between Li-Gc is found in the range of 1.273 to 1.374 Å for first to third H_2 molecule on each Li while the distance between Li-H ranges from 2.036 to 2.065 Å for first to third H_2 molecules adsorbed on each Li in the system. All the distances are provided in Table 1. The hydrogen wt.% is found to be 7.2 for $MGFLi_{16}$-$48H_2$ system, where each Li adsorbs 3 H_2 molecules via physisorption.

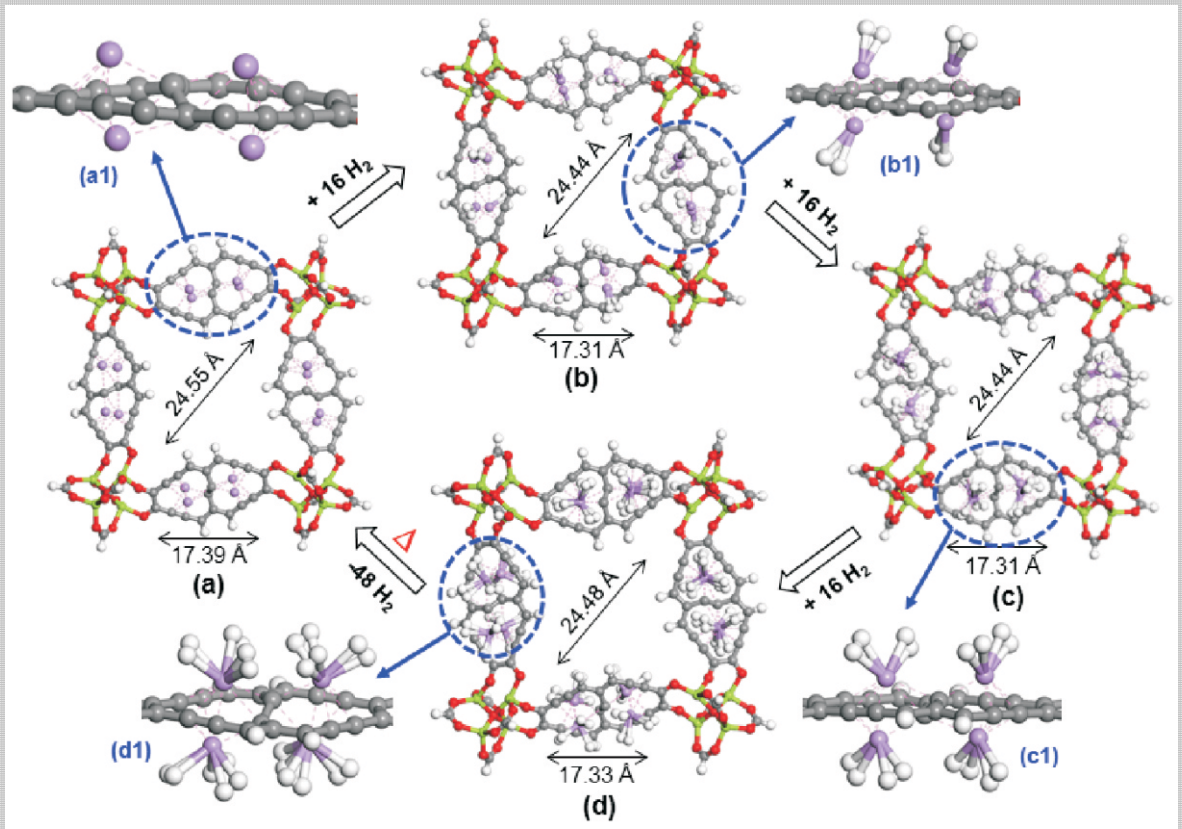

Fig. 2. Hydrogen sorption pathway of (a) $MGFLi_{16}$, (b) $MGFLi_{16}$-$16H_2$, (c) $MGFLi_{16}$-$32H_2$ and (d) $MGFLi_{16}$-$48H_2$ systems. Mg, C, H, O and Li atoms are represented by green, dark grey, white, red and purple colors respectively. For clarity, the enlarged images of linkers are shown in a1, b1, c1 and d1.

Table 1. The average bond distance between Li-Li from top and bottom of the graphyne linker in $MGFLi_{16}$, graphyne center of MGF and Li (Li-Gc), Li and physisorbed hydrogen distance (Li-H) and physisorbed hydrogen distance (H-H). All average distances are measured in Å

System	Li-Li	Li-Gc	Li-H	H-H
$MGFLi_{16}$	2.534	1.267	–	–
$MGFLi_{16}$-$16H_2$	2.547	1.273	2.036	0.755
$MGFLi_{16}$-$32H_2$	2.634	1.317	2.069	0.754
$MGFLi_{16}$-$48H_2$	2.749	1.374	2.065	0.755

The pore space of Li grafted framework is available for more hydrogen molecules storage. To increase the hydrogen storage capacity, 12 more H_2 molecules are introduced in the pore space of $MGFLi_{16,}$ and the optimized resulting geometry of $MGFLi_{16}$-$60H_2$ is shown in Fig. 3. The hydrogen molecules in the pore space trapped with elongation in H-H bond distance. The calculated H wt.% is found to be 8.9 for $MGFLi_{16}$-$60H_2$.

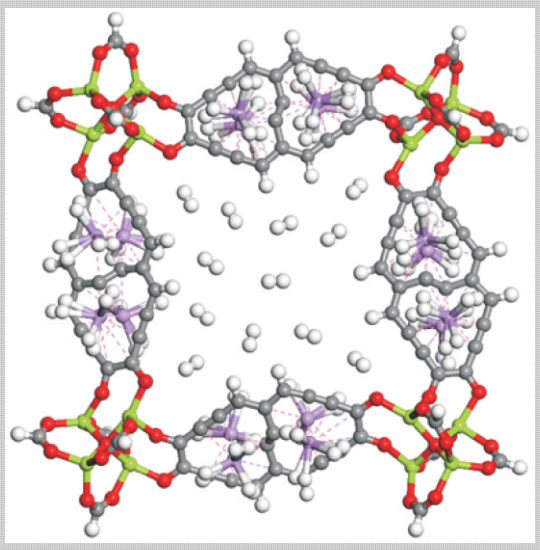

Fig. 3. Optimized structure of $MGFLi_{16}$-$60H_2$. Mg, C, H, O and Li atoms are represented by green, dark grey, white, red, and purple colors respectively.

Energetic parameters

The binding strength of adsorbed H_2 and Li atom of $MGFLi_{16}$ system is explored by computing the average H_2 adsorption energy, E_{ad}, by using eq. (2). The adsorption energy values for first H_2 molecule adsorbed on each Li in $MGFLi_{16}$-nH_2 is found to be 0.36 eV. On further adsorption of second and third H_2 molecules on each Li results in $MGFLi_{16}$-$32H_2$ and $MGFLi_{16}$-$48H_2$ systems and the E_{ad} values are 0.32 and 0.28 eV, respectively for second and third H_2 molecule. The average adsorption energy for 12 more H_2 molecules trapped in the pore space of $MGFLi_{16}$-$48H_2$ is calculated and found between 0.28 to 0.25 eV for 49th to 60th H_2 molecule in the $MGFLi_{16}$-nH_2 (n = 49 to 60). The adsorption energy values for hydrogen molecules trapped in the pore space are provided in Table S1 in the Supporting Information. The adsorption energy values indicate that hydrogen molecules are adsorbed reversibly and these values are found in the desired range of target set by the DOE.

Further, to examine the reversibility of adsorbed H_2 from the Li grafted MGF, the subsequent desorption energy, E_{de}, is calculated by using eq. (3). The desorption energy values are 0.36, 0.29 and 0.21 eV, respectively for first, second and third hydrogen molecules adsorbed in $MGFLi_{16}$-nH_2 (n = 16, 24, and 48) system. The desorption energy values show that the adsorbed hydrogen molecules are easily detached from the Li grafted $MGFLi_{16}$-nH_2 systems. The average H_2 adsorption and subsequent desorption energy values are given in Table 2. These low values of both average hydrogen adsorption and subsequent desorption energies indicate that Li grafted MGF is reversible hydrogen storage material.

Table 2. The average adsorption (E_{ad}) and sequential desorption (E_{de}) energy of adsorbed H_2 molecules in $MGFLi_{16}$-nH_2 (where n = 16, 32, and 48) system. All energy values are given in eV

System	E_{ad}	E_{de}
$MGFLi_{16}$	–	–
$MGFLi_{16}$-$16H_2$	0.36	0.36
$MGFLi_{16}$-$32H_2$	0.32	0.29
$MGFLi_{16}$-$48H_2$	0.28	0.21

Hirshfeld charge analysis of $MGFLi_{16}$-nH_2

The charge transfer mechanism is explored by computing Hirshfeld charges on C atoms of graphyne linker of MGF, on Li atoms before and after hydrogen adsorption and adsorbed hydrogen in the systems. The Hirshfeld charges are computed in e.u. and plotted in Fig. 4. The Hirshfeld charge values are 0.007, –0.015, –0.014, –0.013, and –0.012 e.u. respectively, for C atoms of graphyne linker of MGF, $MGFLi_{16}$, $MGFLi_{16}$-$16H_2$, $MGFLi_{16}$-$32H_2$, and $MGFLi_{16}$-$48H_2$ systems. The Hirshfeld charges on Li atoms are found to be 0.320, 0.239, 0.209, and 0.195 e.u. for Li grafted system and for first, second, and third hydrogen loaded system. Further, the charges on adsorbed hydrogen are 0.034, 0.021, and 0.015 e.u., respectively for first, second, and third hydrogen molecule adsorbed on each Li in the system. It is observed that charge on C atoms of graphyne linker increases up to –0.015 e.u. on Li grafting.

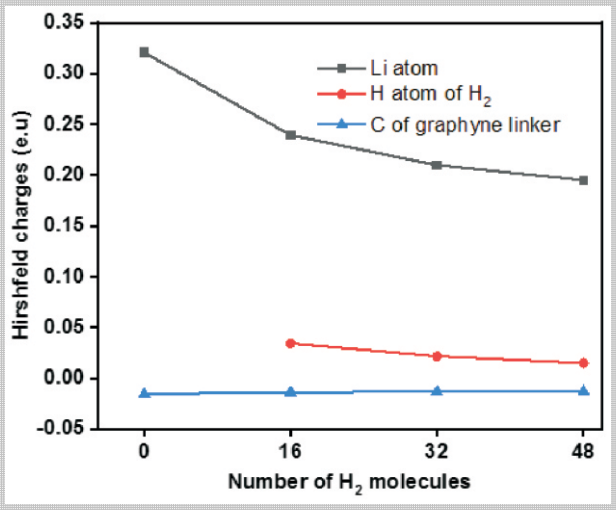

Fig. 4. Hirshfeld charges on C atom of graphyne linker, Li atom and adsorbed hydrogen of $MGFLi_{16}$-nH_2 system (where n = 16, 32, and 48).

The neutral Li donates electronic charge to the C of graphyne linker and gets positive charge on Li grafting MGF. The sequential adsorption of hydrogen molecules on each Li in the system shows Li gets an electronic charge from the C of graphyne linker and H of adsorbed hydrogen molecules. The Hirshfeld charge transfer indicates that the adsorbed hydrogen molecules bind with Li of $MGFLi_{16}$ by charge polarization mechanism.

Thermodynamic usable hydrogen capacity

To be a potential material for hydrogen storage, enough H_2 molecules should be adsorbed at storage conditions and these adsorbed H_2 molecules should be smoothly desorbed

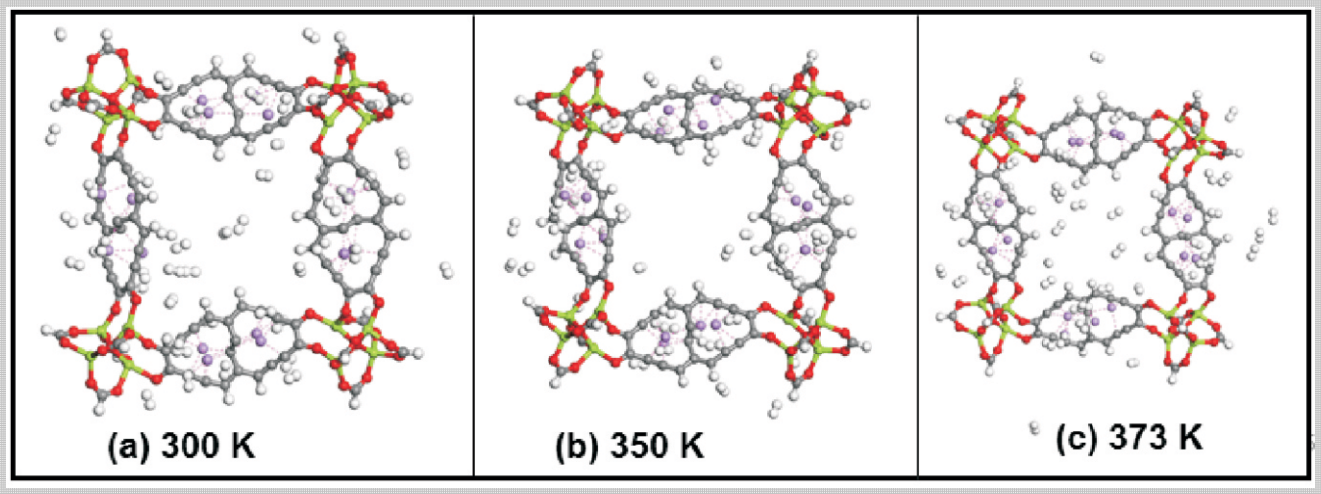

Fig. 5. Snap-shots of BOMD simulations of $MGFLi_{16}$-$48H_2$ at the temperatures of (a) 300, (b) 350 and (c) 373 K.

from the material at desorption conditions. To determine the usable hydrogen capacity, the occupation number (N_{use}) has been calculated by using eq. (4). The operational conditions for H_2 adsorption at adsorption (30 atm and 298 K) and H_2 release at desorption conditions (3 atm and 373 K)[47,48].

The values of μ_{ideal} at 30 atm and 298 K is –0.21 eV which results in the μ value –0.22 eV. However, at 3 atm and 373 K, the μ_{ideal} value is –0.36 eV and the μ value is –0.38 eV. The calculated occupation number, *N*, is found to be 2.25 at adsorption conditions (30 atm and 298 K), and *N* is 0.31 at desorption conditions (3 atm and 273 K). So, the usable number, N_{use}, shows that 1.94 H_2 molecules per Li adsorbed at operational conditions in the Li grafted MGF with the practical H wt.% 5.3.

Molecular dynamics simulations of $MGFLi_{16}$-$48H_2$ system

BOMD simulations have been performed over three different temperatures 300, 350, and 373 K up to 5 ps run time with 1 fs time-step to understand the stability of $MGFLi_{16}$ system and the reversible process of adsorbed hydrogen from the fully hydrogen saturated $MGFLi_{16}$-$48H_2$ system. The snap shots of BOMD simulations are provided in Fig. 5a-c at three different temperatures. The BOMD simulations at 300 K, indicating that hydrogen molecule starts releasing from the $MGFLi_{16}$-$48H_2$ system and one hydrogen molecule from each Li is detached from the system. Further, on increasing the simulation temperature up to 350 K, show that two hydrogen molecules are smoothly released from each Li of $MGFLi_{16}$-$48H_2$. The simulation at a higher temperature up to 373 K shows that all three hydrogen molecules desorbed from each Li of $MGFLi_{16}$-$48H_2$ system. The simulations at 373 K, shows that MGF structure is stable and the Li remains near the graphyne linker in the framework. Simulations at 373 K also show that there is no Li clustering. The study of BOMD simulations reveals that all the hydrogen molecules are adsorbed in a reversible manner which makes $MGFLi_{16}$ as a potential material for hydrogen storage.

Conclusions

The hydrogen storage properties of Li grafted MGF has been explored by using first-principles density functional theory. The GGA-PBE functional along with DNP basis set has been used throughout the calculations. The Li-graphyne binding energy 2.68 eV show that Li strongly binds with graphyne linker of MGF making $MGFLi_{16}$ system. Sequential introduction of hydrogen molecules on Li grafted MGF show that maximum 3 H_2 molecules are adsorbed on each Li in the system and the resulting structure $MGFLi_{16}$-$48H_2$ is obtained. The hydrogen molecules are adsorbed in a molecular manner by charge polarization mechanism indicates that all the hydrogen molecules adsorbed in physisorbed fashion. The calculated average adsorption and sequential desorption energy values are low and found in the range of target set by DOE, i.e. between 0.2–0.4 eV, which confirms that all the adsorbed H_2 molecules are reversible. Hirshfeld charge

analysis further proves that hydrogen molecules are adsorbed by the charge polarization mechanism proposed by Niu-Rao-Jena.

The practical usable hydrogen capacity is calculated as a function of temperature and pressure. The stability of $MGFLi_{16}$ and the release of adsorbed hydrogen molecules from $MGFLi_{16}$-$48H_2$ are examined by BOMD simulations at the temperature range between 300 to 373 K. BOMD simulations indicate that all the hydrogen molecules are liberated at 373 K. The simulations confirm that the structure of $MGFLi_{16}$ is stable up to 373 K which show that the Li grafted MGF can be reused to store the hydrogen molecules. The adsorbed wt.% is found to be 8.9 for hydrogen saturated $MGFLi_{16}$ system which is higher than earlier studied MGF decorated with eight Li atoms[27]. The high weight % and low sorption values for Li decorated system makes it a potential hydrogen storage material.

Acknowledgements

Financial support by the Council of Scientific and Industrial Research (CSIR), New Delhi (CSIR Grant No. 01(2782)14/EMR-II) is gratefully acknowledged. The authors thank IIT Ropar for Interdisciplinary research project for Hydrogen Storage under Renewable and Clean Energy and high-performance computing cluster facility.

Supporting Information

Average H_2 adsorption energy of $MGFLi_{16}$-nH_2 (n = 49-60) are provided in Table S1. The internal coordinates of all the optimized geometries of MGF, $MGFLi_{16}$, $MGFLi_{16}$-nH_2 (n = 16, 32, 48, and 60) are provided in Tables S2-S6 in Supporting Information.

References

1. L. Schlapbach and A. Züttel, *Nature,* 2001, **414**, 353.
2. I. Staffell, D. Scamman, A. A. V. Abad, P. Balcombe, P. E. Dodds, N. Shah and K. R. Ward, *Environ. Sci.,* 2019, **12**, 463.
3. I. Sreedhar, K. M. Kamani, B. M. Kamani, B. M. Reddy and A. Venugopal, *Renew. Sust. Energy Rev.,* 2018, **91**, 838.
4. N. L. Rosi, J. Eckert, M. Eddaoudi, D. T. Vodak, J. Kim, M. O'Keeffe and O. M. Yaghi, *Science,* 2003, **300**, 1127.
5. S. Kumar and T. J. Kumar, *J. Phys. Chem. C,* 2017, **121**, 8703.
6. P. Jena, *J. Phys. Chem. Lett.,* 2011, **2**, 206.
7. J. Graetz, *Chem. Soc. Rev.,* 2009, **38**, 73.
8. A. Dillon, K. M. Jones, T. A. Bekkedahl, C. H. Kiang, D. S. Bethune and M. J. Heben, *Nature,* 1997, **386**, 377.
9. J. Gu, X. Zhang, L. Fu and A. Pang, *Int. J. Hydrogen Energy,* 2019, **44**, 6036.
10. R. H. Baughman, H. Eckhardt and M. Kertesz, *J. Chem. Phys.,* 1987, **87**, 6687.
11. D. Malko, C. Neiss, F. Vines and A. Gorling, *Phys. Rev. Lett.,* 2012, **108**, 086804.
12. P.-P. Liu, H. Zhang, X.-L. Cheng and Y.-J. Tang, *Appl. Surf. Sci.,* 2016, **371**, 44.
13. Y. Guo, K. Jiang, B. Xu, Y. Xia, J. Yin and Z. Liu, *J. Phys. Chem. C,* 2012, **116**, 13837.
14. C. Li, J. Li, F. Wu, S.-S. Li, J.-B. Xia and L.-W. Wang, *J. Phys. Chem. C,* 2011, **115**, 23221.
15. K. Srinivasu and S. K. Ghosh, *J. Phys. Chem. C,* 2012, **116**, 5951.
16. Q. Sun, P. Jena, Q. Wang and M. Marquez, *J. Am. Chem. Soc.,* 2006, **128**, 9741.
17. S. Kumar, R. Y. Sathe and T. J. Dhilip Kumar, *Phys. Chem. Chem. Phys.,* 2017, **19**, 32566.
18. S. Kumar, R. Y. Sathe and T. J. Dhilip Kumar, *Int. J. Hydrogen Energy,* 2019, **44**, 4889.
19. S. Kumar, R. Y. Sathe and T. J. Dhilip Kumar, *Int. J. Hydrogen Energy,* 2019, **44**, 12724.
20. H. Wu, W. Zhou and T. Yildirim, *J. Am. Chem. Soc.,* 2007, **129**, 5314.
21. R. B. Rankin, J. Liu, A. D. Kulkarni and J. K. Johnson, *J. Phys. Chem. C,* 2009, **113**, 16906.
22. S. S. Han, J.-L. Mendoza-Cortes and W. A. Goddard III, *Chem. Soc. Rev.,* 2009, **38**, 1460.
23. A. Blomqvist, C. M. Araujo, P. Srepusharawoot and R. Ahuja, *Proc. Natl. Acad. Sci. USA,* 2007, **104**, 20173.
24. M. Eddaoudi, J. Kim, N. Rosi, D. Vodak, J. Wachter, M. O'Keeffe and O. M. Yaghi, *Science,* 2002, **295**, 469.
25. H. Furukawa, K. E. Cordova, M. O'Keeffe and O. M. Yaghi, *Science,* 2013, **341**, 1230444.
26. K. Sillar, A. Hofmann and J. Sauer, *J. Am. Chem. Soc.,* 2009, **131**, 4143.
27. S. Kumar and T. J. Dhilip Kumar, *ACS Appl. Mater. Interfaces,* 2017, **9**, 28659.
28. Y. Pramudya and J. L. Mendoza-Cortes, *J. Am. Chem. Soc.,* 2016, **138**, 15204.
29. A. P. Cote, A. I. Benin, N. W. Ockwig, M. O'Keeffe, A. J. Matzger and O. M. Yaghi, *Science,* 2005, **310**, 1166.
30. M. Samolia and T. J. Dhilip Kumar, *J. Phys. Chem. C,* 2014, **118**, 10859.
31. S. Kumar, M. Samolia and T. J. Dhilip Kumar, *ACS Appl. Energy Mater.,* 2018, **1**, 1328.
32. K. Gopalsamy and V. Subramanian, *J. Phys. Chem. C,* 2016, **120**, 19932.
33. T. J. Dhilip Kumar, P. F. Weck and N. Balakrishnan, *J. Phys. Chem. C,* 2007, **111**, 7494.

34. The U.S. Department of Energy, Office of Energy Efficiency & Renewable Energy. Target Explanation Document: Onboard Hydrogen Storage for Light-Duty Fuel Cell Vehicles. https://www.energy.gov/sites/prod/files/2017/05/f34/fcto_targets_onboard_hydro_storage_explanation.pdf, accessed on 27/04/2019.
35. D. A. Gomez-Gualdron, Y. J. Colon, X. Zhang, T. C. Wang, Y.-S. Chen, J. T. Hupp, T. Yildirim, O. K. Farha, J. Zhang and R. Q. Snurr, *Energy Environ. Sci.,* 2016, **9**, 3279.
36. D. A. Gomez-Gualdron, T. C. Wang, P. Garcia-Holley, R. M. Sawelewa, E. Argueta, R. Q. Snurr, J. T. Hupp, T. Yildirim and O. K. Farha, A*CS Appl. Mater. Interfaces,* 2017, **9**, 33419.
37. Y. Guo, K. Jiang, B. Xu, Y. Xia, J. Yin and Z. Liu, *J. Phys. Chem. C,* 2012, **116**, 13837.
38. B. Delley, *J. Chem. Phys.,* 1990, **92**, 508.
39. B. Delley, *J. Chem. Phys.,* 2000, **113**, 7756.
40. J. P. Perdew, K. Burke and M. Ernzerhof, *Phys. Rev. Lett.,* 1996, **77**, 3865.
41. S. Grimme, *J. Comput. Chem.,* 2006, **27**, 1787.
42. T. D. Kühne, *Wiley Interdiscip. Rev.: Comput. Mol. Sci.,* 2014, **4**, 391.
43. R. Y. Sathe, S. Kumar and T. J. Dhilip Kumar, *Int. J. Hydrogen Energy,* 2018, **43**, 5680.
44. R. Y. Sathe, S. Kumar and T. J. Dhilip Kumar, *Int. J. Hydrogen Energy,* 2019, **44**, 6663.
45. H. Lee, W. I. Choi, M. C. Nguyen, M. H. Cha, E. Moon and J. Ihm, *Phys. Rev. B,* 2007, **76**, 195110.
46. D. R. Lide, "Handbook of Chemistry and Physics", CRC Press, New York, 1994.
47. J. Niu, B. K. Rao and P. Jena, *Phys. Rev. Lett.,* 1992, **68**, 2277.
48. J. Niu, B. K. Rao and P. Jena, *Phys. Rev. B,* 1995, **51**, 4475.

Special Issue on "Theoretical and Computational Chemistry"

J. Indian Chem. Soc.,
Vol. 96, July 2019, pp. 801-807

Comparison of TDDFT and multireference treatment of ground and excited states of Fe(II) ammonia octahedral complex

Koushik Seth and Debashree Ghosh*

School of Chemical Sciences, Indian Association for the Cultivation of Science,
2A & 2B, Raja Subodh Chandra Mallick Road, Jadavpur, Kolkata-700 032, India

E-mail: pcdg@iacs.res.in

Manuscript received online 21 April 2019, revised and accepted 15 May 2019

Multireference methods and time dependent density functional theory (TDDFT) is used to compute the ground and excited states at different spin states of a prototype spin crossover complex. It is observed that while density functional theory (DFT) with certain functionals can get the energetics of the ground state accurately, multireference treatment is crucial to the proper depiction of the excited states. We have further used a DFT orbital based complete active space self consistent field method to form a computationally affordable alternative. This approach proves to be quite efficient in accurate depiction of the ground and excited states of such complexes.

Keywords: Spin crossover, multireference, Fe(II) ammonia octahedral complex.

Introduction

Spincrossover (SCO) complexes form a very interesting class of transition metal complexes, where the stable spin state of the complex can change with light irradiation, magnetic field, applied pressure or thermal equilibria[1,2]. This change in spin state is accompanied with change in a plethora of physical properties of the complex or material, such as magnetism, optical absorption etc. Fe(II), i.e. $3d^6$ complexes in a nearly octahedral ligand field is known to exhibit such SCO properties[3–5]. This is governed by the fact that the Fe(II) moiety in the octahedral ligand field, shows a d-orbital splitting that gives access to an array of different spin states with small differences in their energies. The SCO complexes were discovered more than 50 years back, and have fascinated researchers due to its obvious material and technological applications in the fields of spintronics and molecular memory storage devices[6–9].

In spite of its immense technological applications, the accurate understanding, prediction and therefore, engineering of SCO molecules and materials are still extremely challenging problems[10]. Fig. 1 shows the schematics for the different spin states of a typical SCO molecule. The two different scenario can give rise to temperature or light induced spin crossover processes. The most stable spin state and

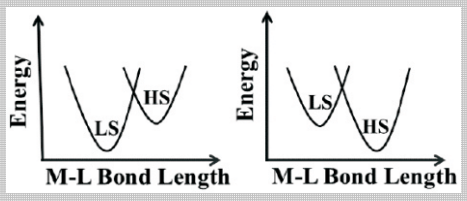

Fig. 1. Schematics of high and low spin state energies at different metal ligand bond lengths. In case of octahedral Fe-N bonded complexes, the high and low spin states are close in energy giving rise to possibility of spin crossover.

the energy differences between the spin states are a combined effect of the central metal ion, ligand field effect as well as other environmental factors, such as counter-ion etc. While experimental techniques such as magnetic susceptibility[11–15] can detect the spin state (or fractional population of the spin states) of the material at a particular temperature, it lacks insight into the electronic structure of the molecule. Ultrafast optical, X-ray or Raman spectroscopies have been used to get a dynamical picture of the structural reorganization[16–20]. Combined with theoretical insights these experimental techniques can indeed prove to be decisive in elucidating the exact mechanism of the spin state changes that are relevant in processes such as light induced excited spin state trapping (LIESST)[21–29].

As mentioned above, the SCO phenomenon relies on the accurate d-orbital splitting of the octahedral complexes. These d-orbital splitting energies are very small in magnitude (< 1.0 eV) and therefore, the accurate estimation of the ligand fields on the splitting is crucial to the prediction of the phenomena[30,31]. Due to the near degeneracies of the d-orbitals at the valence space, computationally these systems are challenging. The wavefunction is multireference in nature and the d-orbitals are strongly correlated with each other. Therefore, state of the art multireference methods need to be applied to understand the electronic structure of the system. Complete active space based methods, such as complete active space self consistent field (CASSCF) have been applied for such systems[23,25]. However, as is well known now, large basis sets and complete information about the large ligands is also crucial which makes these methods quite computationally expensive. Furthermore, it is known that large active space including a few metal-ligand orbitals are required to characterize the ligand field splitting accurately[23]. Dynamic correlation needs to be included either perturbatively or variationally via, complete active space perturbation (CASPT2) or multireference configuration interaction (MRCI). Even for state of the art multireference methods, such as CASPT2, the adiabatic HS-LS gap is overestimated, i.e. it over stabilizes the HS state by about 0.4 eV[27]. This is somewhat higher than the expected chemical accuracy of 0.1 eV. Here, it should be noted that density functional theory (DFT) with several functionals have been used to benchmark the HS-LS gap of these octahedral complexes and it is found and PBE0 and OPBE functionals are best known to reproduce the *ab initio* (wavefunction based) HS-LS gaps[32–36]. Furthermore, there is severe dearth of benchmark experimental results for these quantities due to the difficulty in isolating the moieties. The best theoretical estimates have been developed from a CASPT2 scheme with correction for extra dynamic correlation[23,27].

However, extending this approach to excited states is always fraught with complications. DFT is known to underestimate the charge transfer state energies and therefore, it is expected to overestimate the effect of metal-ligand charge transfer (MLCT) nature of the transitions. This would, therefore, fundamentally change the electronic structure of the states and therefore, use of TDDFT to study the low-lying excited states may indeed give rise to spurious method dependent artefacts.

In this study we have applied active space based methods with increasing active spaces to understand the interplay of the methods and active spaces, to obtain a best estimate value of the ground and excited spin states of Fe(II) octahedral complex. As a prototype nitrogen core based octahedral complex we have chosen $[Fe(NH_3)_6]^{2+}$. The active space methods that are evaluated are CASSCF, CASPT2, *n*-electron valence perturbation (NEVPT2) and MRCI. It is to be noted that MRCI is the most robust of these approaches due to its variational approach of including dynamic correlation as opposed to the perturbative schemes, such as CASPT2 and NEVPT2. However, MRCI is computationally expensive and therefore, in our study we have compared, small active space MRCI to large active space perturbative approaches. We have further developed a computationally efficient DFT orbital based CASCI scheme.

Here, the idea is to include effective dynamic correlation in the DFT orbitals which are then strongly correlated. We compare the accuracy and limitations of this scheme.

Computational details

$[Fe(NH_3)_6]^{2+}$ complex have been optimized at the DFT level with PBE0 functional and TZVP basis set at the singlet, triplet and quintet states. These will be referred to as low spin (LS), intermediate spin (IS) and high spin (HS) states, respectively. Cartesian coordinate of optimized geometries and frequency analysis of all spin states are given in Supporting information.

The linearly interpolated internal coordinate (LIIC) approach is used to generate the structures in between the optimized HS and LS geometries. Here we generate 7 LIIC intermediate structures. These LIIC geometries are used to obtain the potential energy surface (PES) for the ground states at different spin states with PBE0 and B3LYP functionals as well as with active space based methods. Several different active spaces are used to understand its effect. The smallest active space (5o,6e) contains the 6 electrons and the 5d orbitals of the $3d^6$ Fe atom. Next, we include 5 more 4d orbitals that are vacant in the Hartree Fock level, thus making a (10o,6e) active space. It is also reported in the literature that 4s and 3d orbitals are strongly correlated and therefore can lead to significant change in the energetics, therefore an even larger (12o,10e) active space is also investigated. With all these three different active spaces, CASSCF, CASPT2 and NEVPT2 methods are used to cal-

culate the HS-LS energy difference in the ground state. State averaged (SA) CASSCF and multi state (MS) CASPT2 have been used for the ground and excited states, while state specific (SS) NEVPT2 have been used for the ground states. Finally, in order to include more metal ligand correlation at an equal footing a CASSCF of (15o,10e) largest active space is used. We have proposed and tested a DFT orbital based CASCI method for HS-LS energy difference. In this protocol, a PBE0/TZVP level of theory calculation is performed to generate KS orbitals which are then reused for CASCI calculations with appropriate active space.

Excited states with the same levels of theory are compared with the TDDFT (with B3LYP functional) excited states to understand the difference in the energetics and electronic structure of the states as determined by the various theoretical approaches. For the single point ground state and excitation energies quantum chemistry software packages, Q-Chem 5.037 and Molpro 2018[38] were used.

Results and discussion

Structure of the molecule

The optimized HS, LS and IS states of the $[Fe(NH_3)_6]^{2+}$ complex is shown in Fig. 2. As expected, the higher spin states are characterized by longer metal ligand bond lengths (2.28 Å, 2.28 Å and 2.29 Å) as compared to the other spin states. The bond lengths of the IS are 2.07 Å, 2.23 Å and 2.29 Å, and is characterized by maximally different bond lengths with inversion symmetry. The low spin is completely symmetric with 2.09 Å bond length.

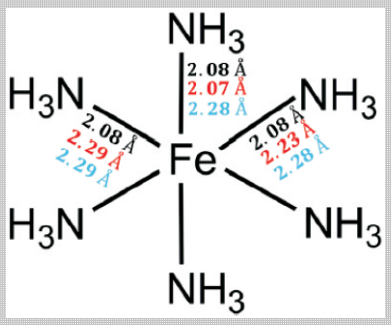

Fig. 2. Optimized structure of $[Fe(NH_3)_6]^{2+}$: black, red and blue colour signify the bond lengths in LS , IS and HS state respectively.

Active space

In complete active space based approaches, the qualitative and quantitative accuracy of the states depend strongly on the choice of the correct active spaces. This is especially true in case of SCO compounds where the different spin states are very close in energy. The orbitals involved in the various active spaces used in our study are shown in Fig. 3.

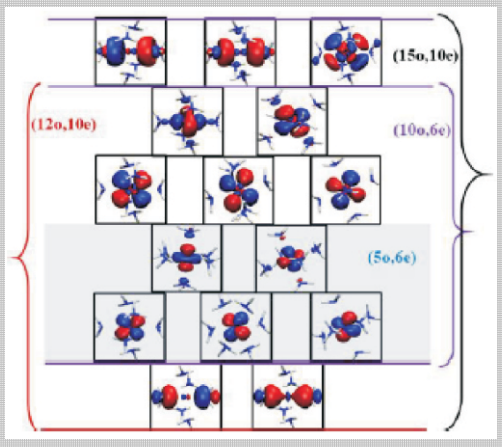

Fig. 3. Orbitals included in different active space.

One would expect naively that the minimal active space containing the most strongly correlated antibonding combination of metal 3d and ligand orbitals would be sufficient to obtain a correct qualitative picture of the spin states. When the metal ligand bonds are considered to be ionic in the limiting case, these orbitals reside completely on the metal. However, these bonds are not completely ionic, they have some covalent contribution and therefore, there are small ligand contributions in these orbitals. Pierloot[23] and co-workers have noted in their studies on 3d and higher transition metal complexes that a double shell effect is important for transition metal ions for those that have more than half filled d shell. They have shown that significant 3d-4s transition is needed to capture the exact energetics of the spin states. In order to include the double shell effect therefore, another 5 vacant 4d orbitals are included in the active space. This double shell effect is included in the (6e,10o) active space. Two e-like σ bonding orbitals are also close energetically to the d-orbitals and can therefore, be strongly correlated, which forms the (10e,12o) active space as shown in Fig. 3. Finally, three ligand virtual orbitals of π^* character are included to capture the correlated metal ligand charge transfer components of the excited states. This forms the largest (10e,15o) active space used in our calculations. This is expected to

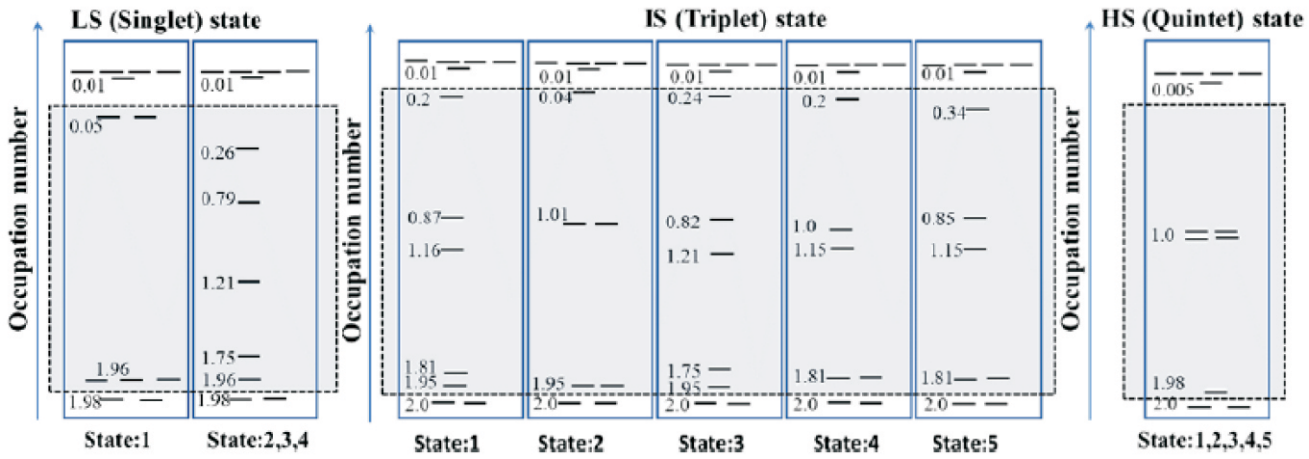

Fig. 4. Natural orbitals occupation number of excited states of HS optimized geometry for different spin states in CASSCF (12o,10e) calculation.

include all strongly correlated orbitals in the full valence space.

One can understand the importance of the different orbitals in the active space from the occupation numbers of the CASSCF natural orbitals. Fig. 4 shows the natural orbital populations of the lowest few excited states. It depicts the relative importance of the orbitals and have been shown only at the high spin optimized geometry.

Ground state

The ground state energy differences between HS and LS states (adiabatic HS-LS energy gap) at different levels of theory are shown in Table 1. It shows that the active spaces (12o,10e) and (15o,10e) are both quite adequate in depicting the energetics of the ground state. This is in accordance with our expectation since the antibonding orbitals on the ligands are not expected to play an important role in the ground state energies as corroborated by the occupation numbers of these orbitals in the ground state. However, these orbitals might well be crucial for higher excited states, especially when these excited states have a mixed MLCT character. Furthermore, we notice that dynamic correlation is important to predict the accurate energy gaps. From earlier work, the best estimate of *ab initio* HS-LS energy gap for the system at the CASPT2 and corrected CASPT2 levels of theory are around 100–131 kJ/mol[23,27]. Our results follow the same observation. As expected from earlier work, PBE0 functional is in reasonable accordance with CASPT2 results with HS-LS gap of 86 kJ/mol[22]. We have also included zero-point energy corrections to get the best estimate of HS-LS gap at 102 kJ/mol, at the DFT level of theory.

Table 1. Energy difference between HS and LS at different levels of theory for various active spaces are shown. The ZPE correction is not included

Active space	Energy differences (LS-HS) (kJ/mol)		
	CASSCF	CASPT2	NEVPT2
(5o,6e)	231	172	133
(10o,6e)	203	162	169
(12o,10e)	134	100	98
(15o,10e)	83	NA	NA

This is compared to the DFT orbital based CASCI protocol. The idea here is to have dynamically correlated orbitals (albeit from DFT) and to include the static correlation from an active space based approach. It should be noted that for large active spaces this method might suffer from double counting of correlation effects. The DFT-CASCI estimate for the adiabatic HS-LS energy difference is 143.80 kJ/mol, as compared to the best estimates of 100–131 kJ/mol. This is indeed quite encouraging, since the DFT-CASCI approach is significantly computationally efficient.

Excited state

While much of the existing literature deals with the comparison of the ground HS-LS states with complete active space based methods and that of DFT based functionals, there is relatively little that is known about the excited states at the different spin states. Table 2 shows the vertical excitation energies (VEEs) at different spin states at the stable HS geometry.